LC-PHSM-2001-022
January 16, 2001

A Study of Charged Current Triple Gauge Couplings at TESLA

Wolfgang Menges

II. Institut für Experimentalphysik, Universität Hamburg
Luruper Chaussee 149, 22761 Hamburg, Germany

Abstract

We present a study of measuring triple gauge couplings in the semileptonic decay channel of the W-pair production at the e^+e^- future linear collider TESLA. A sensitivity in the order of 10^{-3} to 10^{-4} can be reached depending on the coupling under consideration. Beam polarization improves the sensitivity and helps to disentangle WWZ and WWγ couplings. We also investigate some sources of systematic errors.

1 Introduction

Exploring the triple gauge couplings (TGCs) gives the possibility to study the bosonic sector of the standard model (SM) [1–3]. We can verify if the $\mathrm{SU}(2)_L\times\mathrm{U}(1)_Y$ gauge structure of the SM is realized in nature. Deviations from this could indicate a signal for new physics beyond the SM like Supersymmetric (SUSY) Models [4–8] or other extra particles, which alter the TGCs through loop corrections. For example the contributions from SUSY models to TGCs [9] like $\Delta\kappa_\gamma$ can be as high as 5×10^{-3} at a center-of-mass energy of 500 GeV. But this depends on the specific model and set of SUSY parameters. A linear collider at a center-of-mass energy of 500 GeV or higher will deliver enough luminosity to measure TGCs with an accuracy where we can distinguish such effects from the SM predictions.

In this study the expected sensitivity for a measurement of triple gauge couplings is investigated. The expected statistical sensitivity of such a measurement is discussed including the gain of beam polarization. Also the disentanglement of WWZ and WWγ couplings by using polarized beams is addressed. In addition some major systematic errors are estimated based on the TESLA design presented at various workshops on linear colliders and on the TESLA reference detector as described in the CDR [10].

The triple gauge boson couplings are extracted from W-pairs using the spin density matrix method. The aim of this method is to determine the helicity states of the W-bosons as a function of the production angle $\cos\theta_W$. These have a high sensitivity to anomalous triple gauge couplings.

2 Triple Gauge Couplings

The triple gauge boson vertex WWV (V = Z or γ) can be described in a most general form by an effective Lagrangian [11]

$$\begin{aligned}\frac{\mathcal{L}^{WWV}}{ig_{WWV}} &= g_1^V V^\mu\left(W^-_{\mu\nu}W^{+\nu} - W^+_{\mu\nu}W^{-\nu}\right) + \kappa_V W^-_\mu W^+_\nu V^{\mu\nu} + \frac{\lambda_V}{M_\mathrm{W}^2}V^{\mu\nu}W^{+\rho}_\mu W^-_{\rho\nu}\\ &- ig_4^V W^-_\mu W^+_\nu(\partial^\mu V^\nu + \partial^\nu V^\mu)\\ &+ ig_5^V\varepsilon^{\mu\nu\rho\sigma}\left[(\partial^\rho W^-_\mu)W^+_\nu - W^-_\mu(\partial^\rho W^+_\nu)\right]V_\sigma\\ &+ \frac{\tilde\kappa_V}{2}W^-_\mu W^+_\nu\varepsilon^{\mu\nu\rho\sigma}V_{\rho\sigma} + \frac{\tilde\lambda_V}{2M_\mathrm{W}^2}W^-_{\rho\mu}W^{+\mu}{}_\nu\varepsilon^{\nu\rho\alpha\beta}V_{\alpha\beta},\end{aligned}\tag{1}$$

which is parametrised by seven real couplings for each vertex. Their behavior under charge (C) and parity (P) conjugation can be used to divide them into four groups. The three couplings g_1^V,κ_V and λ_V conserve C and P, while g_5^V violates C and P but conserves CP. The couplings g_4^V,$\tilde\kappa_V$ and $\tilde\lambda_V$ violate CP, but g_4^V conserves P, while $\tilde\kappa_V$ and $\tilde\lambda_V$ conserve C. In the SM at tree level the couplings are $g_1^V{=}\kappa_V{=}1$, while all other are set to zero. For convenience we introduce $\Delta g_1^\gamma = g_1^\gamma - 1$, $\Delta g_1^Z = g_1^Z - 1$, $\Delta\kappa_\gamma = \kappa_\gamma - 1$ and $\Delta\kappa_Z = \kappa_Z - 1$ thus we are only considering deviations from the standard model values.

Electro-magnetic gauge invariance requires g_1^γ=1 and reduces the number of C and P conserving couplings to 5. $\mathrm{SU}(2)_L \times \mathrm{U}(1)_Y$ gauge invariance introduces

$$\begin{aligned} \Delta\kappa_\mathrm{Z} &= \Delta\kappa_\gamma \tan\theta_W + \Delta g_1^\mathrm{Z} \\ \lambda_Z &= \lambda_\gamma \end{aligned} \tag{2}$$

for the C and P conserving couplings, where θ_W is the Weinberg angle, thus reducing the number of free couplings further. With this we ensure that possible extensions of the SM have the same structure as the SM.

For the C and P conserving couplings there are two sets to be studied: first the three standard couplings Δg_1^Z,$\Delta\kappa_\gamma$ and λ_γ with relation (2) and second all five couplings Δg_1^Z,$\Delta\kappa_\gamma$,$\Delta\kappa_\mathrm{Z}$,λ_γ and λ_Z without any relation between them. This gives us the possibility to explore further the $\mathrm{SU}(2)_L \times \mathrm{U}(1)_Y$ gauge structure of the standard model. In addition we consider a third set of couplings with all C or P violating WWZ couplings. We do not consider any C or P violating WWγ couplings. There are other processes like single W [12,13] or single γ [14,15] production which are also sensitive to these couplings.

3 W-pair Event Topology

A W boson can decay either into a charged lepton and a neutrino or into two quarks. This gives three decay channels for WW pairs: the leptonic ($\mathcal{BR}$=0.10), the semileptonic ($\mathcal{BR}$=0.43) and the hadronic ($\mathcal{BR}$=0.47) decay channel. The event can be fully described by five angles, ignoring finite width effects and initial state radiation (ISR). Figure 1 shows the W production angle θ_W, which is the angle between the incoming electron and the outgoing W^-, and the four decay angles $\cos\theta^*_{1,2}$ and $\phi^*_{1,2}$, two for each W boson. The two decay angles $\cos\theta^*$ and ϕ^* describe the direction of the down-type fermion f_d in the rest frame of the W. This is sufficient because both decay fermions are back-to-back in this frame.

Not all three decay channels can be fully reconstructed from the measured particles. In the $l\bar{\nu}_l\bar{l}\nu_l$ channel all five angles can only be reconstructed by assuming energy and momentum conservation and forcing both W bosons to the same, fixed mass. These six constrains help to reconstruct the two unmeasured neutrinos. This is only true for events with no taus in the final state. Events with one or two taus are rejected because they can not be reconstructed due to the further neutrinos from the tau decays. The five angles can be reconstructed up to a twofold ambiguity because a quadratic equation must be solved. In the four quark channel there is the problem of the right combination from jets to Ws. The charge and thus the sign of $\cos\theta_W$ can be partly estimated by using a jet-charge method. But without flavor tagging no information about the flavor of the jets is available and an ambiguity in the assignment of the flavor is left for each W. In the semileptonic channel the reconstruction is much easier. The two jets are assigned to one W and the charged lepton to the other. This gives also the charges of the W bosons. Only for tau events some special care is needed because the tau decays in the detector and only the decay products without the neutrino are measured. But with some assumptions the tau can be reconstructed from its decay products. Like in the four quark channel without

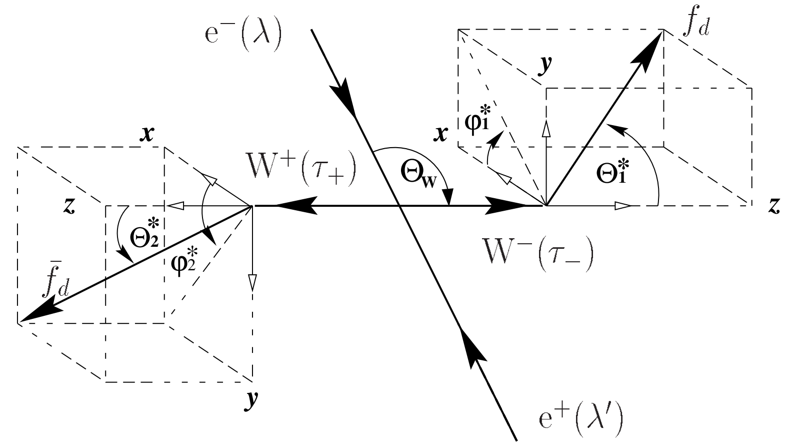

Figure 1: Definition of the five W pair angles and helicities.

flavor tagging an ambiguity in the hadronic decay angles $\cos\theta_j^*$ and ϕ_j^* is left over and only folded distributions can be measured. Because the quark and the anti-quark are back-to-back the ambiguity is $(\cos\theta_j^*, \phi_j^*) \leftrightarrow (-\cos\theta_j^*, \phi_j^* + \pi)$. The folding will be done as follows

$$\begin{aligned} \cos\theta_j^* > 0 \quad &\rightarrow \quad (\cos\theta_j^*,\, \phi_j^*) \\ \cos\theta_j^* < 0 \quad &\rightarrow \quad (-\cos\theta_j^*,\, \phi_j^* + \pi) \end{aligned} \tag{3}$$

Anomalous couplings alter the production and helicity structure of W-pairs with respect to the standard model. Therefore the $\cos\theta_W$ distribution and any observable related to the helicity structure of the Ws can be used to extract information about anomalous couplings. The spin density matrix represents the helicity states of the Ws and is discussed in more detail in the next section.

4 Spin Density Matrices

The spin density matrix (SDM) elements [16] are normalized products of the helicity amplitudes [11] and describe the polarization of the W boson pair. The elements of the two-particle joint density matrix are defined by

$$\rho_{\tau_-\tau'_-\tau_+\tau'_+}(\cos\theta_W) = \frac{\sum\limits_{\lambda} \mathcal{F}^{(\lambda)}_{\tau_-\tau_+} (\mathcal{F}^{(\lambda)}_{\tau'_-\tau'_+})^*}{\sum\limits_{\lambda\tau_+\tau_-} |\mathcal{F}^{(\lambda)}_{\tau_-\tau_+}|^2}, \tag{4}$$

where $\mathcal{F}^{(\lambda)}_{\tau_-\tau_+}$ is the helicity amplitude for a given electron helicity λ and W-pair helicity τ_- and τ_+. With the normalization

$$\sum_{\tau_+,\tau_-} \rho_{\tau_-\tau_-\tau_+\tau_+} = 1 \tag{5}$$

the W^+W^- system has 80 independent SDM elements. This number can be reduced by considering only one-particle density matrices, one for each W boson. The one-particle SDM for one W boson is defined as the sum of the two-particle SDM over all helicity states of the other W

$$\begin{aligned} \rho^{W^-}_{\tau_-\tau'_-}(\cos\theta_W) &= \sum_{\tau_+} \rho_{\tau_-\tau'_-\tau_+\tau_+} \\ \rho^{W^+}_{\tau_+\tau'_+}(\cos\theta_W) &= \sum_{\tau_-} \rho_{\tau_-\tau_-\tau_+\tau'_+}. \end{aligned} \tag{6}$$

Using only one-particle spin density matrices, which is the case in this study, neglects the spin correlations between the different W bosons. The resulting lose in sensitivity is expected to be small. With the normalization

$$\sum_{\tau} \rho^{W^-}_{\tau\tau} = 1, \qquad \sum_{\tau} \rho^{W^+}_{\tau\tau} = 1 \tag{7}$$

the number of independent elements is reduced to nine for each W boson. The one-particle spin density matrix is hermitian and thus the diagonal elements $\rho^{W^\pm}_{\tau\tau}$ are real. They can be interpreted as the probability to produce a $W^\pm$ boson with the helicity τ. The off-diagonal elements can be complex and describe interference effects between different helicity states.

In CP-conserving theories the imaginary part of the off-diagonal elements must vanish. This follows directly from the properties of the helicity amplitudes under CPT and CP transformations and is described in reference [17] in more detail. On the other hand the imaginary part of the off-diagonal elements are three CP-odd observables, which are very useful for the investigation of CP-odd anomalous couplings. Figure 3 shows the three imaginary parts of the off-diagonal elements for the two anomalous couplings $\tilde{\kappa}_Z = 1$ and $\tilde{\lambda}_Z = 1$ at Born-level.

The SDM elements are extracted from data[1] using projection operators [18]. The three-fold differential cross section can be expressed as the production cross section multiplied by the sum of all SDM elements

$$\begin{aligned} \frac{d^3\sigma(e^+e^- \to W^+ + f\bar{f}')}{d\cos\theta_W d\cos\theta^*_{W^-} d\phi^*_{W^-}} &= \frac{d\sigma(e^+e^- \to W^+W^-)}{d\cos\theta_W} \\ & Br\frac{3}{8\pi}\sum_{\tau_-\tau'_-} \rho^{W^-}_{\tau_-\tau'_-}(\cos\theta_W) D_{\tau_-\tau'_-}(\cos\theta^*,\phi^*), \end{aligned} \tag{8}$$

where Br is the branching ratio of the $W^+f\bar{f}'$ channel and $D_{\tau\tau'}$ the so-called D-function, which describe the angular dependence of the W decay $W^- \to f\bar{f}'$. This equation can be solved for

[1] In this kind of study Monte Carlo events are used as fake data.

the SDM elements by using appropriate projection operators. The matrix element of a certain bin k of $\cos\theta_W$ can be obtained by

$$\rho^k_{\tau\tau'} = \frac{1}{N_k}\sum_{i=1}^{N_k} \Lambda_{\tau\tau'}(\theta^*_i, \phi^*_i), \tag{9}$$

where N_k is the number of events in bin k and θ^*_i and ϕ^*_i are the decay angles of the ith event. The projection operators $\Lambda_{\tau\tau'}$ are given by

$$\begin{aligned}
\Lambda^{\mathrm{W}+}_{\pm\pm} &= \Lambda^{\mathrm{W}-}_{\mp\mp} &&= \tfrac{1}{2}(5\cos^2\theta^* \mp 2\cos\theta^* - 1)\\
\Lambda^{\mathrm{W}+}_{00} &= \Lambda^{\mathrm{W}-}_{00} &&= 2 - 5\cos^2\theta^*\\
\Lambda^{\mathrm{W}+}_{+-} &= \Lambda^{\mathrm{W}-}_{-+} &&= 2\exp(2i\phi^*)\\
\left(\Lambda^{\mathrm{W}+}_{\mp 0}\right)^* &= -\Lambda^{\mathrm{W}-}_{\pm 0} &&= \tfrac{8}{3\pi\sqrt{2}}(1 \mp 4\cos\theta^*)\exp(\mp i\phi^*).
\end{aligned} \tag{10}$$

Figure 4 shows the real parts of the SDM elements for the SM and an anomalous coupling of $\Delta g^{\mathrm{Z}}_1 = 0.1$.

5 Analysis

For this study we assume a luminosity of $500\,\mathrm{fb}^{-1}$ at a center-of-mass energy of 500 GeV, which is the expected amount of data after one or two years of running. For 800 GeV this corresponds to a luminosity of $1000\,\mathrm{fb}^{-1}$. At both energies we expect roughly 4 millions W-pair events. This huge amount of events give us the possibility to do high precision measurements of the TGCs.

The semileptonic decay channel ($\mathrm{WW} \to \mathrm{q}\overline{\mathrm{q}}l\bar{\nu}_l$) is used, because of the high branching ration of 43 % and the good event reconstruction. There is only one ambiguity in the hadronic decay angles. From LEP analysis [19] we know that the background is very small.

All signal Monte Carlo samples were generated by WOPPER [20], which is a W-pair generator for CC03 or CC11 diagrams including ISR and beamstrahlung via CIRCE [21]. The CC03 diagram class includes the s-channel γ and Z^0 exchange and the t-channel ν exchange. The CC11 diagram class includes in addition to the CC03 diagrams also single or non-resonant diagrams. Event generation with polarized electron and positron beams is possible which is not a common feature for Monte Carlo generators. The matrix element calculations from WOPPER are used to obtain weights for the reweighting angle distribution as functions of anomalous TGCs. The background samples were generated by PYTHIA [22] also including ISR and beamstrahlung.

For the simulation of the proposed detector design we use the fast simulation program SIMDET (version 3.02 [23]), which is based on the proposed detector design, described in the TESLA CDR [10]. It includes a tracking and calorimeter simulation and a reconstruction of energy-flow objects.

Data Selection at 500 GeV

The selection of the semileptonic channel is a simple cut based selection. It requires one charged lepton and two jets, which should be conform with a W. Missing energy and momentum is required due to the unmeasured neutrino. Further cuts are applied to reject the background, which is dominated by the two-fermion process $Z/\gamma^* \to q\overline{q}$ and four-fermion processes like single-W and single Z production.

The preselection rejects events with less than five charged tracks. Further the transverse momentum must be greater than 5 GeV to account for the missing momentum due to the neutrino and the visible mass, m_{vis}, must be greater than 100 GeV in order to reject radiative returns from the process $Z/\gamma^* \to f\overline{f}$.

The main selection is splitted up into two parts. One for the selection of electrons or muons, which also includes the decays of taus into electrons or muons, and one for the decay of taus into hadrons:

Electron and muon selection:

Each event is searched for an electron or muon with an energy of more than 10 GeV and a separation of more than 5° to the next energy-flow object. The rest of the event is then clustered into two jets. The hadronic W is reconstructed from the two jets and the leptonic W from the lepton and the missing energy vector, assuming momentum conservation. The charge of the Ws is assigned from the lepton charge. The invariant masses m_{W_l} and m_{W_j} of the leptonic and hadronic W are good variables for background suppression. For example a misidentified event from the process $WW \to q\bar{q}'q''\bar{q}'''$ has a large hadronic invariant mass, because all tracks except one are assigned to the hadronic W. To reject single-W and single-Z production m_{W_l} must be less than 150 GeV and to suppress misidentified events from $WW \to q\bar{q}'q''\bar{q}'''$ m_{W_j} must be less than 150 GeV. For further rejection of four fermion background $\cos\theta_W$ should be greater than -0.95.

The prompt decays $WW \to q\overline{q}e\overline{\nu}_e$ or $WW \to q\overline{q}\mu\overline{\nu}_\mu$ are distinguished from the decay of taus into electrons or muons by considering a χ^2 variable constructed from the visible energy divided by the center-of-mass energy, the lepton energy divided by the beam energy and the mass of the leptonic decaying Wdivided by the nominal W mass. The χ^2 is the quadratic sum of the three variables. Candidates with a χ^2 smaller than 1 are classified as tau decays.

For τ candidates the direction of the visible decay products is almost the direction of the τ, because of its high boost. Hence the direction of the visible decay products is taken as the τ direction and the energy is calculated from considering momentum and energy conservation. The missing energy vector for the neutrino is recalculated afterwards. This approach is used for example by the OPAL collaboration in their TGC analysis [19].

Hadronic selection:

Each event is clustered into three jets. It must require at least one low multiplicity jet ($N_{track} < 10$) with no high-energy electron or muon ($E > 10$ GeV). If only one low-multiplicity jet is found, it is taken as the τ candidate and the other two jets are assigned to the hadronic W. Otherwise the three jets are arranged in turns into a τ candidate and two jets from the hadronic W. The combination is chosen which give a mass for the hadronically decaying W nearest to the W mass. The τ candidate is reconstructed as described above. Further the τ energy must be greater than 10 GeV. The charge of the Ws is assign from the sum of the charged tracks of the tau candidate. A event with zero charge is rejected. For background suppression both W-masses must be less than 150 GeV and $\cos\theta_W$ greater than -0.95.

At 500 GeV the signal is selected with an efficiency of 61.8 % and a purity of 94.7 %. The electron efficiency with 62.9 % is lower than the reconstruction efficiency for muons (70.3 %) while the tau efficiency is 55.9 %. The main background is the process $e^+e^- \to Ze^+e^-$. See table 1 for a detailed account on the selection efficiencies for the signal and background channels.

For comparison the efficiency for a LEP analysis of this kind is around 80 % with a background contribution around 5 %. See ref. [19], for example. In this cut based selection the efficiency can easily be enhanced by loosening some cuts, but on the other side the background contribution grows. A higher efficiency can probably be achieved by using a more sophisticated method like a likelihood selection [19].

Figure 5 show the measured distributions for the five angles and figure 6 the achieved resolutions for the TESLA detector. The $\cos\theta_W$ resolution is more than one order of magnitude better than what is achieved at LEP [24]. The resolution of the four decay angles $\cos\theta^*$ and ϕ^* are still by a factor of two to three better. This is due to the excellent performance of the TESLA detector.

Fit Method

For the extraction of the TGCs from the measured angles we use a simple χ^2 fit. As input variables we use the normalized $\cos\theta_W$-distribution and the SDM-elements. The total cross section is not used even though it is sensitive to TGCs. For this reason the normalized $\cos\theta_W$-distribution is used in order to drop all cross section information. But the information from a cross section measurement can easily be combined with the results from this measurement. The reference distributions as a function of the anomalous TGCs are obtain by a reweighting technique. Each Monte Carlo event i is weighted by a weight

$$w_i = \frac{\mathrm{d}\sigma^{ano}}{\mathrm{d}\Omega} / \frac{\mathrm{d}\sigma^{SM}}{\mathrm{d}\Omega}, \tag{11}$$

where $\mathrm{d}\Omega = \mathrm{d}\cos\theta_W \mathrm{d}\cos\theta^*_{\mathrm{W-}} \mathrm{d}\phi^*_{\mathrm{W-}} \mathrm{d}\cos\theta^*_{\mathrm{W+}} \mathrm{d}\phi^*_{\mathrm{W+}}$. This is the ratio of the five folded differential cross section for the set of anomalous couplings under consideration to the SM differential cross section. The weight is calculated from the Born-level information and can be applied to either Born-level or fully simulated distributions, hence including detector effects.

This fit method is simple and easy to use. Fits with more than one free variable are no problem.

Also detector effects and selection efficiencies are included by reweighting angle distributions including detector simulation.

6 Unpolarized Beams

In the case of unpolarized beams we expect a luminosity of $500\,\mathrm{fb}^{-1}$ at a center-of-mass energy of 500 GeV and $1000\,\mathrm{fb}^{-1}$ at 800 GeV in one or two years of running. For the extraction of the TGCs we use the normalized $\cos\theta_W$-distribution and the SDM-elements.

Results

Table 3.a) shows the expected statistical error for the different couplings from a 1d-fit at 500 and 800 GeV. A 1d-fit means that only one coupling is allowed to vary freely and all other are set to their Standard Model values. The fit results are arranged into three groups. The first group include the three C and P conserving couplings Δg_1^Z,$\Delta\kappa_\gamma$ and λ_γ with the $\mathrm{SU}(2)_L\times\mathrm{U}(1)_Y$ relations. In the second group the $\mathrm{SU}(2)_L\times\mathrm{U}(1)_Y$ relations are dropped and all five C and P conserving couplings are considered. The last group includes the four C or P violating couplings g_4^Z,g_5^Z,$\tilde{\kappa}_Z$ and $\tilde{\lambda}_Z$.

At 500 GeV the expected errors at generator-level for Δg_1^Z,$\Delta\kappa_\gamma$ and λ_γ are $6-7\times10^{-4}$. Dropping the $\mathrm{SU}(2)_L\times\mathrm{U}(1)_Y$ relation increases the errors of $\Delta\kappa_Z$, λ_γ and λ_Z a bit and of Δg_1^Z by a factor of five while the error of $\Delta\kappa_\gamma$ decreases. The error of the C or P violating couplings ranges between 11×10^{-3} and 86×10^{-3}.

Further the fits were done at generator- and at detector-level (with and without background) to learn more about the simulation of detector and background. A selection efficiency of 61.8 % means an increase of the statistical error by 27 % with respect to the results at generator-level, assuming that the statistical error is proportional to the square root of the number of events. But comparing generator-level with detector-level without including background (table 3.a)) shows that the statistical error increases on average only by 6 %. This means that the data selection rejects mainly events which are not very sensitive to TGCs. Naively one would suspect that the selection efficiency is higher for a TGC sensitive phase space region, but the differential efficiency distributions in $\cos\theta_W$, $\cos\theta_1^*$ and $\cos\theta_2^*$ are almost flat. This effect is not understood from first principles and will be addressed in a more detailed study. Further studies on the different decay channels show that the increase of around 6 % is mainly due to the tau reconstruction. The difference between generator- and detector-level considering electron or muon candidates only is very small. This is due to the excellent resolution of all measured particles specially the electron or muon. But for tau candidates the results differ up to 20 %. This is due to the non optimal tau reconstruction. The approximation of the tau direction by the direction of the visible tau decay products is very good but the tau energy must be calculated from energy and momentum conservation. This calculated energy has a better resolution than the energy from the decay products but is still not optimal. This results in a worse decay angle resolution compared to electron and muon candidates. But the resolution can be improved for example by using a kinematic fit in the event reconstruction. Assuming energy and momentum conservation and constraining both W-masses to be equal give enough constraints to get a better resolution of the tau energy. But the inclusion of background is a more severe problem. The expected errors increase by around 24 % with respect to generator-level and some fit results are not in the range of expected error, which is not the expected behavior. This can be due to a few things. First it could be a real effect. The background peaks around ± 1 in $\cos\theta_W$. This is not so important in the forward region because the signal peaks there also and is dominant. But the backward region is very sensitive to anomalous couplings and the number of expected events is not very high. This means that the background is destroying some of the sensitivity to anomalous couplings, although the signal purity is very high and the background known very well. Another explanation could be the background scaling. For all non-WW backgrounds only 2 million events including detector simulation were generated and then scaled to the expected number of events. For example this scaling factor is around five for the 2-fermion background. The scaling factor is also considered in the error calculation and this increases the error significantly in the backward region and thus destroy the sensitivity, which is in this case a statistical problem. This must be studied in more detail to find the answer to this problem.

This shows that effects from selection and detector simulation are small and well understood. A more sophisticated selection method and a better tau reconstruction can reduce the difference between generator- and detector-level up to a few percent. The background inclusion is to be understood totally and some more work must be done on this topic. Nevertheless for all further fits only the generator-level is considered.

At 800 GeV we gain a factor up to two in sensitivity with respect to 500 GeV. The size of the data sample changes only a little bit with energy, but anomalous effects described by an effective theory are more pronounced at higher energies. We also see that we lose sensitivity by discarding the $\mathrm{SU}(2)_L \times \mathrm{U}(1)_Y$-relation (2). The sensitivity for the C or P violating couplings is almost an order of magnitude worse than the sensitivity for the standard couplings.

The high luminosity of TESLA give us the opportunity to explore the correlation between the couplings with high precision in a multi dimensional fit. This means that n variables are left free to vary and the rest are set to the standard model values. Tables 4 to 6 show the expected sensitivity and correlation matrix for different combinations of couplings at 500 and 800 GeV. At both energies we have roughly the same behavior.

The behavior of the three standard couplings (with $\mathrm{SU}(2)_L \times \mathrm{U}(1)_Y$ relation (2)) are shown in table 4. The correlation between Δg_1^Z and $\Delta\kappa_\gamma$ is almost 100 % while the correlation between λ_γ and the other two are small. This has a great impact on the expected sensitivity for the 3d-fit. The sensitivity for λ_γ hardly changes while it increases of a factor of four to seven for the other two couplings.

The statistics and the sensitivity of this process is high enough to discard the $\mathrm{SU}(2)_L \times \mathrm{U}(1)_Y$-relation. Table 5 shows the expected sensitivity and correlation matrix for all five C and

P conserving couplings. The fit of five couplings at the same time seems feasible but the correlation between corresponding WWZ and WWγ couplings is very high. This is no surprise, because the structure of the corresponding couplings is the same for unpolarized beams. The high correlation between Δg_1^Z and $\Delta\kappa_\gamma$ in the three parameter fit is due to this high correlation. Equation (2) couples Δg_1^Z with the two couplings $\Delta\kappa_\gamma$ and $\Delta\kappa_Z$. As before the sensitivity for the 5d-fit blows up with respect to the 1d-fit because of the high correlation between different couplings.

Table 6 shows the results for the four C or P violating couplings. We see that the couplings with different properties under C and P transformation are almost not correlated and the expected errors for four free couplings is the same as for one free coupling, except for $\tilde{\kappa}_Z$ and $\tilde{\lambda}_Z$, which have the same transformation properties. The correlation between them is around 50 %.

Systematic Error Sources

First tests for the evaluation of possible systematic uncertainty sources have been carried out. We consider radiative corrections like initial state radiation (ISR) and beamstrahlung and uncertainties in other measurement like the W-mass and the beam energy, which might have an impact on this measurement. Table 7 summaries the results of this study.

The effect of radiative corrections are investigated in a very simple way. For ISR we compare the results of the standard fit with the results of a fit without ISR and assign the shift as the systematic error. For this we switch off the ISR correction in the data distributions and leaving the reweighting distributions unchanged. This corresponds to a change of 100 %. If we require that this error should not dominate the measurement and assuming a linear effect, we need an understanding of ISR in the order of 1 %. The same is done for beamstrahlung. As a rule of thumb we need an understanding of beamstrahlung effects up to 10 % in order to have a systematic error of maximal the expected statistical error. Both requirements are realistic and can be achieved in the next few years. Also beamstrahlung can be studied very well from Bhabha scattering in the forward region [25].

The more standard systematic error sources are discussed next. For the effect of the W-mass on this measurement M_W is changed by ± 50 MeV in the data distributions and the biggest shift between this measurement and the standard measurement is assigned as the systematic error. For the beam energy uncertainties E_{beam} is changed by $10^{-5} \times E_{\mathrm{beam}}$ and the biggest shift between this and the standard measurement is assign as the systematic error. Both sources of uncertainties are small compared to the statistical error and decrease a bit with an increase in the center-of-mass energy.

The last column of table 7 summaries the systematic errors for the different couplings. All errors are combined quadratically and the above discussed goals for ISR (1 %) and beamstrahlung (10 %) are assumed. In total this measurement is not dominated by systematics.

7 Polarized Beams

Beam polarization is very interesting for W-pair production. It gives the possibility to alter the production process for the needs of the measurement. Not only the cross section can be increased or decreased but also the production and decay angle distributions are modified.

In W-pair production the total cross section is calculated from the cross section for left-handed electrons σ_L and right-handed electrons σ_R weighted by the polarizations for electrons and positrons:

$$\sigma = \frac{1}{4}(1 - \mathcal{P}^+)(1 + \mathcal{P}^-)\sigma_R + \frac{1}{4}(1 + \mathcal{P}^+)(1 - \mathcal{P}^-)\sigma_L. \tag{12}$$

σ_L includes all three CC03-diagrams while σ_R only the two s-channel diagrams. This is shown in figure 2. The ν-diagram vanishes because the charged current does not couple to right-handed electrons. The unpolarized cross section is dominated by the contribution from σ_L. It is 160 times larger than σ_R at 500 GeV and 90 times larger at 800 GeV.

The polarization of electrons and positrons allows us to alter the mixing of both contributions with respect to the unpolarized case. For $\mathcal{P}^- = +1$ only σ_R contributes to the total cross section, for $\mathcal{P}^- = -1$ only σ_L. This contribution is enhanced by a factor of two $(1+\mathcal{P}^-)$ with respect to the contribution for the unpolarized case. The use of additional positron polarization further enhances the total cross section by a factor of $(1 + \mathcal{P}^+)$. This give an additional factor of two for $\pm 100\,\%$ polarization. This give us the novel opportunity to switch off the irreducible background from the ν-diagram and look only at signal-diagrams. Additional the weight of the Z-diagram depends on polarization of the fermion which couple to the Z boson, which is shown in figure 2. The contribution from the photon-diagram is independent of the polarization. This allows to disentangle the contributions from WWZ- and WWγ-vertex.

For the linear collider TESLA the electron polarization will be $\pm 80\,\%$. The positron polarization is more difficult to achieve, but $\pm 60\,\%$ should be reachable. In this case the ν-diagram can not

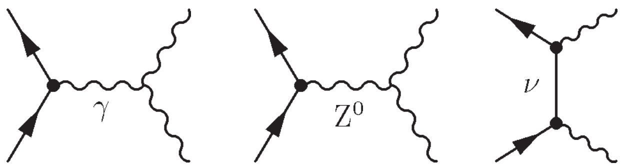

(a) left-handed electrons

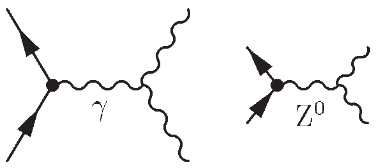

(b) right-handed electrons

Figure 2: Dominant diagrams for left-handed and right-handed electrons which contribute to the W-pair production.

be switched off in total but the contribution can be suppressed or enhanced. For left polarized electrons the enhancement factor is still $(1+\mathcal{P}^+)(1-\mathcal{P}^-)$, which give a factor of roughly 2.5 for electron and positron polarization. But it is different with right polarized electrons because σ_R is much smaller than σ_L. The total cross section is dominated by σ_L. The suppression factor is roughly five for electron polarization only. The positron polarization decreases the total cross section further by a factor of two in contrast to the above discussed increase of $1+\mathcal{P}^+$.

For a given polarization also the differential distributions are changed with respect to the unpolarized case in the SM, which can not be distinguished a priori from an anomalous coupling. Thus it is very important to know the exact polarization.

For studies with polarized beams the $\cos\theta_W$-distribution and the SDM-elements are used as input variables for the fit. The total luminosity for one center-of-mass energy is split up equally on both polarizations. In the case of electron polarization this is for an energy of 500 GeV 250 fb^{-1} on left-handed (L) and 250 fb^{-1} on right-handed (R) electrons with a polarization of 80 %. In the case of additional polarized positrons the absolute value is 60 % with opposite polarization with respect to the electron polarization.

To get the maximal sensitivity for this measurement the data taken at both polarization combinations are fitted at the same time. Only this ensures that we can disentangle the WWZ from the WWγ couplings.

Results

Table 3.b) and c) show the expected statistical error for electron and electron/positron polarization at a center-of-mass energy of 500 and 800 GeV for a 1d fit. At 500 GeV the statistical error decreases by a factor of $1.5-2.5$ using both electron and positron polarization. The gain from using no polarization to using electron polarization only is roughly the same from using electron polarization to using electron and positron polarization. This is a bit different at 800 GeV. The total gain from no beam polarized to both beams is still the same but some couplings gain more from only electron polarization than from electron and positron polarization and vice versa. Still the expected errors at 800 GeV are better than at 500 GeV. This shows that both beams at the highest achievable degree of polarization are best for this kind of measurement, but already a polarized electron beam helps very much.

For both polarization cases fits with more than one free parameter have been done. The results are shown in table 4 to 6. In the case of the three C and P conserving couplings with the $\mathrm{SU}(2)_L\times\mathrm{U}(1)_Y$ relations the use of polarized beams removes the high correlation between Δg_1^{Z} and $\Delta\kappa_\gamma$. At 500 GeV all three couplings are correlated moderately. At an energy of 800 GeV they are hardly correlated anymore. But the main point of using polarized beams is to disentangle the five C and P conserving Z- and γ-couplings. For both beams polarized the correlation for example between $\Delta\kappa_\gamma$ and $\Delta\kappa_{\mathrm{Z}}$ is around 20 % at both energies and the correlation between λ_γ and λ_Z roughly 60 % at 500 GeV and vanishes at 800 GeV. Using only electron polarization is already sufficient to reduce the correlation significantly. For the four C

or P violating couplings the use of polarized electrons or positrons is only needed to increase the sensitivity. The couplings are hardly correlated except $\tilde{\kappa}_Z$ and $\tilde{\lambda}_Z$. The use of polarized beams does not help to further decrease this correlation.

Polarization Errors

As mentioned above it is very important to know the exact polarization because deviation from the expected polarization can fake a contribution from an anomalous coupling. The measurement of the polarization will be performed by a polarimeter using either compton scattering [26] or Møller scattering [27]. For both methods a relative error of $\Delta\mathcal{P}/\mathcal{P} = 0.5{-}1.0\%$ are reachable.

To estimate the systematic error in the TGC measurement from the uncertainty in the polarization measurement the polarization is changed by $\Delta P = \pm 1\,\%$ in the data samples leaving the reweighting samples unchanged. From the different possible combinations of changing the polarization the largest shift is used as an estimate of the systematic error for the polarization uncertainty.

Table 8 shows the systematic errors for 500 and 800 GeV and for both polarization options. At an energy of 500 GeV all measurements are dominated by the polarization error. This error is $5 - 10$ times greater than the statistical error. At the higher energy the behavior is more mixed. Some couplings are almost not affected by the polarization error but others are. This is more pronounced in the case of electron and positron polarization. From this observations a polarization error of $\Delta P = 0.1 - 0.2\,\%$ is needed for a measurement which is not dominated by this polarization error. This translate into the following relative errors for electron polarization $\Delta\mathcal{P}^-/\mathcal{P}^- = 0.1 - 0.2\,\%$ and positron polarization $\Delta\mathcal{P}^+/\mathcal{P}^+ = 0.2 - 0.3\,\%$.

One way out of a high precision polarization measurement with a polarimeter is the simultaneous measurement of the polarization and the TGCs. This is discussed in the next section.

Blondel Scheme

Polarization can be measured from cross section asymmetries. Such a scheme was first proposed by A. Blondel for the case of LEP [28]. K. Mönig proposed [29] to use such a scheme at linear collider energies to improve the accuracy of the polarization measurement for various physical analysis. The idea is to measure the polarization simultaneously with the anomalous couplings. The relevant variables for the polarization measurement are the cross sections at the different helicity combinations of the beams. There are two combinations in the case of electron polarization and four in the case of electron and positron polarization. In the later case the combinations where the beams have the same helicity are needed because otherwise there are not enough variables to constrain the measurement.

For this simultaneous measurement the total cross section is very important. The normalized differential distributions are not sensitive enough to measure the polarization preciously enough, specially for left-handed electrons. But the cross sections of the different helicity combinations help to improve this significantly.

The total cross section σ_{rew} as a function of anomalous couplings for different polarization schemes is calculated by

$$\sigma_{rew} = \frac{\sigma_{gen}}{N_{gen}} \sum_i w_i, \tag{13}$$

where w_i is the weight for event i as a function of anomalous couplings. σ_{gen} is the cross section and N_{gen} the number of events of the Monte Carlo sample, which is reweighted. This approximates the true cross section very well.

For the simultaneous measurement of TGCs and polarization the total cross section for the different helicity states of the beams is used as an input for the fit in addition to the normalized $\cos\theta_W$ distribution and the SDM elements. The polarization has been fitted simultaneously with the anomalous couplings and a free normalization at a center-of-mass energy of 800 GeV for only electron polarization and electron and positron polarization. In both cases the polarizations can be measured very accurately and the correlation between polarization and TGC measurement is maximal 30 %. This means that the sensitivity of the couplings decreases only a little.

The stability of this method against changes in the polarization is not yet studied. Interesting is the behavior for changes in the absolute polarization and if the absolute value of the polarization for opposite sign helicity states is not the same. A more detailed study is needed to see if this method really helps to control the systematic errors from polarization uncertainties. Then the question can be answered if we need a very high precision polarimeter or not.

8 Electroweak Symmetry Breaking

In the absence of a light Higgs particle or other light resonances, unitarity requires that gauge boson self-interactions becomes strong at high energies. In this case, the physics of electro weak symmetry breaking (EWSB) below the symmetry breaking scale $\Lambda \approx 3\,\text{TeV}$ is described by the most general effective Lagrangian for Goldstone bosons required by $\mathrm{SU}(2)_L \times \mathrm{U}(1)_Y \rightarrow \mathrm{U}(1)_Q$ breaking. Tree-level calculations show that the ρ-parameter is unity in the Standard Model. Deviations from unity measured by LEP1/SLC can be accounted for by loop corrections. This suggests that the EWSB sector appears to have an approximate global $\mathrm{SU}(2)_c$ custodial symmetry, which constrains the ρ-parameter to unity. This symmetry is only broken by the hypercharge couplings to the Goldstone bosons. Thus it is reasonable to investigate possible $\mathrm{SU}(2)_c$-conserving deviations from the SM in the first place.

Assuming only $\mathrm{SU}(2)_L \times \mathrm{U}(1)_Y \rightarrow \mathrm{U}(1)_Q$ symmetry breaking, the most general effective Lagrangian effecting TGCs contains three dimension-four interactions. The corresponding operators of this Lagrangian [30–33] are

$$\begin{aligned} L_1 &= \tfrac{\alpha_1}{16\pi^2}\tfrac{gg'}{2} B_{\mu\nu}\,\mathrm{tr}\Big(\sigma_3 W^{\mu\nu}\Big) \\ L_2 &= \tfrac{\alpha_2}{16\pi^2}\mathrm{i}g' B_{\mu\nu}\,\mathrm{tr}\Big(\sigma_3 V^\mu V^\nu\Big) \\ L_3 &= \tfrac{\alpha_3}{16\pi^2}2\mathrm{i}g\,\mathrm{tr}\Big(W_{\mu\nu} V^\mu V^\nu\Big), \end{aligned} \tag{14}$$

where L_3 conserves the approximate $\mathrm{SU}(2)_c$, while L_1 and L_2 break it linearly. The coefficients α_i are related to scales of new physics Λ_i^* by naive dimensional analysis [34–36]

$$\frac{\alpha_i}{16\pi^2} = \left(\frac{v}{\Lambda_i^*}\right)^2 \tag{15}$$

where the Fermi scale $v = 246\,\mathrm{GeV}$ is fixed by low energy weak interactions.

Couplings

The standard anomalous TGCs are related to the coefficients of the effective Lagrangian by

$$\begin{aligned} g_1^Z &= 1 + \frac{e^2}{\cos^2\theta_w(\cos^2\theta_w - \sin^2\theta_w)}\frac{\alpha_1}{16\pi^2} + \frac{e^2}{\sin^2\theta_w\cos^2\theta_w}\frac{\alpha_3}{16\pi^2} \\ \kappa_Z &= 1 + \frac{2e^2}{\cos^2\theta_w - \sin^2\theta_w}\frac{\alpha_1}{16\pi^2} - \frac{e^2}{\cos^2\theta_w}\frac{\alpha_2}{16\pi^2} + \frac{e^2}{\sin^2\theta_w}\frac{\alpha_3}{16\pi^2} \\ \kappa_\gamma &= 1 - \frac{e^2}{\sin^2\theta_w}\frac{\alpha_1}{16\pi^2} + \frac{e^2}{\sin^2\theta_w}\frac{\alpha_2}{16\pi^2} + \frac{e^2}{\sin^2\theta_w}\frac{\alpha_3}{16\pi^2}\,. \end{aligned} \tag{16}$$

The transformation (16) is singular and the three anomalous TGCs satisfy

$$(\Delta g_1^{\mathrm{Z}} - \Delta\kappa_{\mathrm{Z}}) \cdot \cos^2\theta = \Delta\kappa_\gamma \cdot \sin^2\theta. \tag{17}$$

Only two dimensions of the α parameter space can be determined directly in the W-pair production. The blind direction

$$(\alpha_1,\ \alpha_2,\ \alpha_3)_{\mathrm{blind}} \propto (\cos^2\theta_w - \sin^2\theta_w,\ \cos^2\theta_w,\ -\sin^2\theta_w) \tag{18}$$

in the parameter space can not be constrained from the three TGCs alone, but additional measurements of α_1 can be used to solve this. For example the oblique corrections ΔS depend on α_1 and can be measured at LEP1/SLC. For convenience we fit α_2 and α_3 and take the SM value $\alpha_1 = 0$.

Results

The results for a two dimensional fit of α_2 and α_3 with $\alpha_1 = 0$ is shown in table 9 for both energies and different combinations of polarized beams. In the case of unpolarized beams α_2

and α_3 are strongly correlated, but fortunately this can be suppressed already with electron polarization. Using additional positron polarization suppresses the correlations even further. For both beams polarized, figure 9 shows the contour plot for an energy of 800 GeV. For this case expected errors are $\Delta\alpha_2 = 0.09$ and $\Delta\alpha_3 = 0.048$.

These sensitivities can be interpreted by equation (15) as limits on scales of new physics Λ_i^* described by the corresponding operator in the effective Lagrangian (14). See table 9 for explicit numbers. In the case of no polarization only energies around the symmetry breaking scale of 3 TeV can be probed. But with the use of polarized beams energies well above the symmetry breaking scale of 3 TeV can be probed. The best limits are 10.3 TeV for Λ_2^* and 14.1 TeV for Λ_3^* at an energy of 800 GeV and both beams polarized.

9 Conclusion

We show that an expected error of the order of 10^{-3} to 10^{-4} depending on the coupling under consideration is feasible. Some sources of systematic errors have been investigated. There are no major problems expected from the uncertainties from the W mass or the beam energy. Also radiative corrections like ISR and beamstrahlung seem to be under control.

Detector effects and selection issues like efficiency and purity have been studied in more detail for a center-of-mass energy of 500 GeV. The excellent performance of the TESLA detector can be seen from the very good resolution of the production angles θ_{W} and the four decay angles. Specially the resolution of $\cos\theta_W$ is one order of magnitude better than a LEP detector.

Fitting TGCs with detector simulation also shows the good resolution of the TESLA detector. Considering only electron or muon candidates the expected errors increase only a few percent. The not optimal tau reconstruction is more of a draw-back but the expected errors increase on average only by 6 % considering the whole signal. This is very interesting because statistical arguments suggest an increase of around 27 % with respect to the generator-level assuming a selection efficiency of 61.8 %. But the background inclusion is not well understood. On average the expected errors increase by 24 % with respect to the generator-level. It is not clear if this is a real effect or due to an insufficient amount of simulated background.

Further the use of polarized beams is investigated. The use of electron polarization helps to increase the sensitivity to anomalous TGCs and gives the opportunity to disentangle the WWZ from the WWγ couplings which are highly correlated in the case of no beam polarization. The use of a polarized positron beam enforce this two points. In the case of polarized beams the knowledge of the exact polarization is very important. The systematic error from varying the absolute polarization by 1 % dominates the measurement of all couplings. This require an excellent polarimeter with an absolute error of $0.1 - 0.2$ % or the simultaneous measurement of the polarization with the TGCs. Such a measurement can be done with a Blondel Scheme using all available polarization combinations. The polarization can be measured very accurately and with almost no correlation with the TGCs. But the stability of this method must be investigated in more detail.

Acknowledgments

I would like to thanks Thorsten Ohl and Klaus Mönig for the useful discussions on this subject. Also the Graduiertenkolleg ”Zukünftige Entwicklungen in der Teilchenphysik” for financial support.

References

[1] S. Weinberg. A Model of Leptons. *Phys. Rev. Lett.*, 19:1264–1266, 1967.

[2] S. L. Glashow. Partial Symmetries of Weak Interactions. *Nucl. Phys.*, 22:579–588, 1961.

[3] A. Salam. Weak and Electromagnetic Interactions. pages 367–377, 1968. Originally printed in *Svartholm: Elementary Particle Theory, Proceedings Of The Nobel Symposium Held 1968 At Lerum, Sweden*.

[4] H. P. Nilles. Supersymmetry, Supergravity and Particle Physics. *Phys. Rept.*, 110:1, 1984.

[5] Howard E. Haber and G. L. Kane. The Search for Supersymmetry: Probing Physics beyond the Standard Model. *Phys. Rept.*, 117:75, 1985.

[6] R. Barbieri, I. Ferrante, F. Fidecaro, M. Frigeni, and J. F. Grivaz. Supersymmetry Searches. In *Geneva 1989, Proccedings, Z physics at LEP 1, vol. 2* 121-145.

[7] J. M. Frere and G. L. Kane. On the Possibility of Finding Light Uncolored Supersymmetric Partners at Present and Future Machines. *Nucl. Phys.*, B223:331, 1983.

[8] John Ellis, J. S. Hagelin, D. V. Nanopoulos, and M. Srednicki. Search for Supersymmetry at the anti-p p Collider. *Phys. Lett.*, B127:233, 1983.

[9] A. Arhrib, J. L. Kneur, and G. Moultaka. MSSM Radiative Contributions to the WWγ and WWZ Form Factors. *Phys. Lett.*, B376:127–135, 1996.

[10] R. Brinkmann, G. Materlik, J. Rossbach, and A. Wagner. Conceptual Design of a 500-GeV e^+e^- Linear Collider with Integrated X-Ray Laser Facility. Vol. 1-2. DESY-97-048::V.1.

[11] K. Hagiwara, R. D. Peccei, D. Zeppenfeld, and K. Hikasa. Probing the Weak Boson Sector in $e^+e^- \to W^+W^-$. *Nucl. Phys.*, B282:253, 1987.

[12] Giampiero Passarino. Unstable Particles and Non-Conserved Currents: A Generalization of the Fermion-Loop Scheme. *Nucl. Phys.*, B574:451–494, 2000.

[13] Michael A. Doncheski, Stephen Godfrey, and K. Andrew Peterson. Single W Boson Production in High Energy e gamma Collisions. 1997.

[14] Debajyoti Choudhury, Jan Kalinowski, and Anna Kulesza. CP-Violating Anomalous W W gamma Couplings in e+ e- Collisions. *Phys. Lett.*, B457:193–201, 1999.

[15] Debajyoti Choudhury and Jan Kalinowski. Unravelling the WWgamma and WWZ vertices at the Linear Collider: Anti-nu nu gamma and anti-nu nu anti-q q Final States. *Nucl. Phys.*, B491:129–146, 1997.

[16] M. Bilenkii, J. L. Kneur, F. M. Renard, and D. Schildknecht. Trilinear Couplings among the Electroweak Vector Bosons and their Determination at LEP200. *Nucl. Phys.*, B409:22–68, 1993.

[17] G. Gounaris, D. Schildknecht, and F. M. Renard. Genuine Tests of CP Invariance in $e^+e^- \to W^+W^-$. *Phys. Lett.*, B263:291–297, 1991.

[18] G. Gounaris, J. Layssac, G. Moultaka, and F. M. Renard. Analytic Expressions of Cross-Sections, Asymmetries and W Density Matrices for $e^+e^- \to W^+W^-$ with General Three Boson Couplings. *Int. J. Mod. Phys.*, A8:3285–3320, 1993.

[19] G. Abbiendi et al. Measurement of Triple Gauge Boson Couplings from W^+W^- Production at LEP Energies up to 189 GeV. 2000.

[20] Harald Anlauf, Panagiotis Manakos, Thorsten Ohl, and Hans Dieter Dahmen. WOPPER, version 1.5: A Monte Carlo Event Generator for $e^+e^- \to W^+W^- \to 4f(n)\gamma$ at LEP2 and Beyond. 1996.

[21] Thorsten Ohl. CIRCE version 1.0: Beam Spectra for Simulating Linear Collider Physics. *Comput. Phys. Commun.*, 101:269–288, 1997.

[22] Torbjorn Sjostrand et al. High-Energy-Physics Event Generation with PYTHIA 6.1. 2000.

[23] M. Pohl and H. J. Schreiber. SIMDET - Version 3: A parametric Monte Carlo for a TESLA Detector. DESY-99-030.

[24] W. Menges. Measurement of the Trilinear Gauge Boson Couplings with the OPAL Detector at LEP. DESY-THESIS-2000-025.

[25] K. Mönig. Measurement of the Differential Luminosity using Bhabha events in the Forward-Tracking region at TESLA. 2000. LC-PHSM-2000-60-TESLA.

[26] P. Schüler. Polarimeter Studies for TESLA. 2000. Talk at the International Workshop on Linear Colliders, Fermilab 24 - 28 October 2000, to appear in the proceedings.

[27] Gideon Alexander and Iuliana Cohen. Møller Scattering Polarimetry for High Energy e^+e^- Linear Colliders. 2000.

[28] Alain Blondel. A Scheme to Measure the Polarization Asymmetry at the Z Pole in LEP. *Phys. Lett.*, B202:145, 1988.

[29] K. Mönig. The use of Positron Polarization for Precision Measurements. 2000. LC-PHSM-2000-59-TESLA.

[30] Thomas Appelquist and Claude Bernard. Strongly Interacting Higgs Bosons. *Phys. Rev.*, D22:200, 1980.

[31] Anthony C. Longhitano. Heavy Higgs Bosons in the Weinberg-Salam Model. *Phys. Rev.*, D22:1166, 1980.

[32] Anthony C. Longhitano. Low-Energy Impact of a Heavy Higgs Boson Sector. *Nucl. Phys.*, B188:118, 1981.

[33] Thomas Appelquist and Guo-Hong Wu. The Electroweak Chiral Lagrangian and CP Violating Effects in Technicolor Theories. *Phys. Rev.*, D51:240–250, 1995.

[34] Steven Weinberg. Phenomenological Lagrangians. *Physica*, A96:327, 1979.

[35] Aneesh Manohar and Howard Georgi. Chiral Quarks and the Nonrelativistic Quark Model. *Nucl. Phys.*, B234:189, 1984.

[36] Howard Georgi and Lisa Randall. Flavor Conserving CP Violation in Invisible Axion Models. *Nucl. Phys.*, B276:241, 1986.

A Tables

Process	σ[pb]	ϵ[%]	N	N[%]
WW $\to q\bar{q}l\bar{\nu}_l$	3.51	61.8	1085166	94.66
WW $\to q\bar{q}'q''\bar{q}'''$	3.71	0.07	1299	0.11
WW $\to l\bar{\nu}_l\bar{l}\nu_l$	0.81	0.05	203	0.02
$q\bar{q}$	21.02	0.18	18918	1.65
ZZ	0.67	1.50	5025	0.44
Ze^+e^-	14.68	0.34	24956	2.18
$We\nu$	6.34	0.34	10778	0.94

Table 1: Selection efficiencies for signal and background at 500 GeV.

energy	polarization	*RL*	*R*	–	*L*	*LR*
500 GeV	$\mathcal{P}^- = \pm 1.0$, $\mathcal{P}^+ = \pm 1.0$	32.1	16.0	8.1	0.1	0.2
	$\mathcal{P}^- = \pm 0.8$, $\mathcal{P}^+ = \pm 0.6$	23.1	14.4	8.1	1.7	0.8
800 GeV	$\mathcal{P}^- = \pm 1.0$, $\mathcal{P}^+ = \pm 1.0$	18.1	9.0	4.6	0.1	0.2
	$\mathcal{P}^- = \pm 0.8$, $\mathcal{P}^+ = \pm 0.6$	12.0	8.1	4.6	1.0	0.5

Table 2: Total cross section for different polarization combinations at a center-of-mass energies of 500 and 800 GeV. The polarization combinations are described by R (right) and L (left). One letter denotes electron polarization only, two letter electron and positron polarization.

	$\Delta g_1^{Z\mathrm{a}}$	$\Delta\kappa_\gamma{}^{\mathrm{a}}$	$\lambda_\gamma{}^{\mathrm{a}}$	Δg_1^Z	$\Delta\kappa_\gamma$	λ_γ	$\Delta\kappa_Z$	λ_Z	g_4^Z	g_5^Z	$\tilde{\kappa}_Z$	$\tilde{\lambda}_Z$
500 GeV[b]	7.3	5.7	6.1	38.1	4.8	12.1	8.7	11.5	85.8	27.7	64.9	11.4
500 GeV[c]	7.8	5.7	6.8	47.5	4.8	13.9	9.0	12.8	82.4	28.7	64.4	11.9
500 GeV[d]	8.6	6.3	8.2	54.0	5.3	18.0	10.0	15.8	86.5	30.7	72.7	14.6
800 GeV[b]	4.5	3.1	2.8	39.0	2.6	5.2	4.9	5.1	41.8	28.5	29.6	4.9

(a) no beam polarization

	$\Delta g_1^{Z\mathrm{a}}$	$\Delta\kappa_\gamma{}^{\mathrm{a}}$	$\lambda_\gamma{}^{\mathrm{a}}$	Δg_1^Z	$\Delta\kappa_\gamma$	λ_γ	$\Delta\kappa_Z$	λ_Z	g_4^Z	g_5^Z	$\tilde{\kappa}_Z$	$\tilde{\lambda}_Z$
500 GeV[b]	4.3	4.2	5.1	24.8	4.1	8.2	5.0	8.9	79.9	22.8	50.6	10.3
800 GeV[b]	2.7	2.3	3.1	21.9	2.2	5.0	2.9	4.7	31.8	24.3	24.1	4.4

(b) electron beam polarization only

	$\Delta g_1^{Z\mathrm{a}}$	$\Delta\kappa_\gamma{}^{\mathrm{a}}$	$\lambda_\gamma{}^{\mathrm{a}}$	Δg_1^Z	$\Delta\kappa_\gamma$	λ_γ	$\Delta\kappa_Z$	λ_Z	g_4^Z	g_5^Z	$\tilde{\kappa}_Z$	$\tilde{\lambda}_Z$
500 GeV[b]	2.8	3.1	4.3	15.5	3.3	5.9	3.2	6.7	45.9	16.5	39.0	7.5
800 GeV[b]	1.8	1.9	2.6	12.6	1.9	3.3	1.9	3.0	18.3	14.4	14.3	3.0

(c) electron and positron beam polarization

[a]With $SU(2)_L \times U(1)_Y$ relations.
[b]Generator-level
[c]Detector-level (without background)
[d]Detector-level (with background)

Table 3: Expected sensitivity ($\times 10^{-4}$) for different couplings at a center-of-mass energy of 500 and 800 GeV and a luminosity of 500 fb^{-1} and 1000 fb^{-1}. In the case of polarized beams the luminosity is split up equally on both combinations.

	$1d$	$3d$	Δg_1^Z	$\Delta\kappa_\gamma$	λ_γ
Δg_1^Z	7.3	34.0	1.000	−0.968	−0.253
$\Delta\kappa_\gamma$	5.7	22.9		1.000	0.173
λ_γ	6.1	6.6			1.000

(a) 500 GeV, no polarization

	$1d$	$3d$	Δg_1^Z	$\Delta\kappa_\gamma$	λ_γ
Δg_1^Z	4.5	34.2	1.000	−0.987	−0.223
$\Delta\kappa_\gamma$	3.1	18.4		1.000	0.198
λ_γ	2.9	3.0			1.000

(b) 800 GeV, no polarization

	$1d$	$3d$	Δg_1^Z	$\Delta\kappa_\gamma$	λ_γ
Δg_1^Z	4.3	4.3	1.000	0.043	−0.282
$\Delta\kappa_\gamma$	4.2	4.6		1.000	−0.215
λ_γ	5.1	5.5			1.000

(c) 500 GeV, e^- polarization (R+L)

	$1d$	$3d$	Δg_1^Z	$\Delta\kappa_\gamma$	λ_γ
Δg_1^Z	2.7	2.4	1.000	−0.082	−0.101
$\Delta\kappa_\gamma$	2.3	2.4		1.000	−0.061
λ_γ	3.1	2.9			1.000

(d) 800 GeV, e^- polarization (R+L)

	$1d$	$3d$	Δg_1^Z	$\Delta\kappa_\gamma$	λ_γ
Δg_1^Z	2.8	3.1	1.000	0.403	−0.383
$\Delta\kappa_\gamma$	3.1	3.5		1.000	−0.299
λ_γ	4.3	4.6			1.000

(e) 500 GeV, e^+e^- polarization (RL+LR)

	$1d$	$3d$	Δg_1^Z	$\Delta\kappa_\gamma$	λ_γ
Δg_1^Z	1.8	1.7	1.000	−0.020	−0.095
$\Delta\kappa_\gamma$	1.9	2.0		1.000	−0.047
λ_γ	2.6	2.4			1.000

(f) 800 GeV, e^+e^- polarization (RL+LR)

Table 4: Expected sensitivity ($\times 10^{-4}$) at generator-level and correlation matrix for an one and three parameter fit. The $SU(2)_L \times U(1)_Y$ relation is used in the fit.

	$1d$	$5d$	Δg_1^Z	$\Delta\kappa_\gamma$	λ_γ	$\Delta\kappa_Z$	λ_Z
Δg_1^Z	38.1	76.6	1.000	0.496	−0.097	−0.609	−0.189
$\Delta\kappa_\gamma$	4.8	33.4		1.000	−0.072	−0.981	−0.073
λ_γ	12.1	25.7			1.000	0.043	−0.818
$\Delta\kappa_Z$	8.7	85.7				1.000	0.112
λ_Z	11.5	22.8					1.000

(a) 500 GeV, no polarization

	$1d$	$5d$	Δg_1^Z	$\Delta\kappa_\gamma$	λ_γ	$\Delta\kappa_Z$	λ_Z
Δg_1^Z	39.0	53.7	1.000	−0.048	−0.189	−0.018	−0.021
$\Delta\kappa_\gamma$	2.6	38.8		1.000	0.311	−0.995	−0.245
λ_γ	5.2	9.6			1.000	−0.304	−0.781
$\Delta\kappa_Z$	4.9	50.5				1.000	0.245
λ_Z	5.1	9.0					1.000

(b) 800 GeV, no polarization

	$1d$	$5d$	Δg_1^Z	$\Delta\kappa_\gamma$	λ_γ	$\Delta\kappa_Z$	λ_Z
Δg_1^Z	24.8	45.2	1.000	0.006	0.263	−0.781	−0.544
$\Delta\kappa_\gamma$	4.1	4.7		1.000	−0.316	−0.185	0.100
λ_γ	8.2	11.7			1.000	−0.139	−0.536
$\Delta\kappa_Z$	5.0	8.4				1.000	0.280
λ_Z	8.9	12.2					1.000

(c) 500 GeV, e^- polarization (R+L)

	$1d$	$5d$	Δg_1^Z	$\Delta\kappa_\gamma$	λ_γ	$\Delta\kappa_Z$	λ_Z
Δg_1^Z	21.9	26.6	1.000	−0.068	0.235	−0.523	−0.445
$\Delta\kappa_\gamma$	2.2	2.4		1.000	−0.044	−0.245	−0.016
λ_γ	5.0	4.8			1.000	−0.162	−0.229
$\Delta\kappa_Z$	2.9	3.2				1.000	0.208
λ_Z	4.7	4.9					1.000

(d) 800 GeV, e^- polarization (R+L)

	$1d$	$5d$	Δg_1^Z	$\Delta\kappa_\gamma$	λ_γ	$\Delta\kappa_Z$	λ_Z
Δg_1^Z	15.5	30.0	1.000	−0.212	0.525	−0.784	−0.722
$\Delta\kappa_\gamma$	3.3	3.6		1.000	−0.362	0.232	0.151
λ_γ	5.9	11.0			1.000	−0.404	−0.649
$\Delta\kappa_Z$	3.2	5.5				1.000	0.434
λ_Z	6.7	12.0					1.000

(e) 500 GeV, e^+e^- polarization (RL+LR)

	$1d$	$5d$	Δg_1^Z	$\Delta\kappa_\gamma$	λ_γ	$\Delta\kappa_Z$	λ_Z
Δg_1^Z	12.6	15.9	1.000	−0.109	0.235	−0.432	−0.449
$\Delta\kappa_\gamma$	1.9	2.1		1.000	−0.020	−0.237	−0.021
λ_γ	3.3	3.3			1.000	−0.173	0.059
$\Delta\kappa_Z$	2.0	2.1				1.000	0.187
λ_Z	3.0	3.3					1.000

(f) 800 GeV, e^+e^- polarization (RL+LR)

Table 5: Expected sensitivity ($\times 10^{-4}$) at generator-level and correlation matrix for an one and five parameter fit.

	$1d$	$4d$	g_4^Z	g_5^Z	$\tilde{\kappa}_Z$	$\tilde{\lambda}_Z$
g_4^Z	85.8	88.4	1.000	−0.026	0.276	−0.048
g_5^Z	27.7	27.7		1.000	−0.002	0.013
$\tilde{\kappa}_Z$	64.9	75.0			1.000	0.445
$\tilde{\lambda}_Z$	11.4	13.1				1.000

(a) 500 GeV, no polarization

	$1d$	$4d$	g_4^Z	g_5^Z	$\tilde{\kappa}_Z$	$\tilde{\lambda}_Z$
g_4^Z	41.8	41.4	1.000	0.013	0.140	−0.024
g_5^Z	28.5	28.4		1.000	−0.035	0.016
$\tilde{\kappa}_Z$	29.6	35.1			1.000	0.531
$\tilde{\lambda}_Z$	4.9	5.9				1.000

(b) 800 GeV, no polarization

	$1d$	$4d$	g_4^Z	g_5^Z	$\tilde{\kappa}_Z$	$\tilde{\lambda}_Z$
g_4^Z	79.9	71.1	1.000	0.013	−0.362	−0.219
g_5^Z	22.8	23.5		1.000	0.200	0.089
$\tilde{\kappa}_Z$	50.6	59.9			1.000	0.517
$\tilde{\lambda}_Z$	10.3	10.7				1.000

(c) 500 GeV, e^- polarization (R+L)

	$1d$	$4d$	g_4^Z	g_5^Z	$\tilde{\kappa}_Z$	$\tilde{\lambda}_Z$
g_4^Z	31.8	32.2	1.000	0.017	0.030	−0.028
g_5^Z	24.3	23.9		1.000	−0.031	−0.013
$\tilde{\kappa}_Z$	24.1	29.8			1.000	0.613
$\tilde{\lambda}_Z$	4.4	5.5				1.000

(d) 800 GeV, e^- polarization (R+L)

	$1d$	$4d$	g_4^Z	g_5^Z	$\tilde{\kappa}_Z$	$\tilde{\lambda}_Z$
g_4^Z	42.7	45.9	1.000	−0.102	−0.410	−0.362
g_5^Z	16.5	16.7		1.000	−0.108	−0.045
$\tilde{\kappa}_Z$	39.0	40.7			1.000	0.662
$\tilde{\lambda}_Z$	7.5	10.1				1.000

(e) 500 GeV, e^+e^- polarization (RL+LR)

	$1d$	$4d$	g_4^Z	g_5^Z	$\tilde{\kappa}_Z$	$\tilde{\lambda}_Z$
g_4^Z	18.3	18.6	1.000	−0.007	−0.053	−0.038
g_5^Z	14.4	14.4		1.000	−0.014	−0.009
$\tilde{\kappa}_Z$	14.3	18.2			1.000	0.618
$\tilde{\lambda}_Z$	3.0	3.8				1.000

(f) 800 GeV, e^+e^- polarization (RL+LR)

Table 6: Expected sensitivity ($\times 10^{-4}$) at generator-level and correlation matrix for an one and four parameter fit.

coupling	ISR 100 %	beamstrahlung 100 %	$M_{\rm W}$	$E_{\rm beam}$	systematic[a] error	statistic error
$\Delta g_1^{\rm Z b}$	302.3	31.0	2.1	1.2	5.0	7.3
$\Delta\kappa_\gamma{}^{\rm b}$	829.1	18.0	1.7	1.1	8.7	5.7
$\lambda_\gamma{}^{\rm b}$	97.6	9.2	0.4	0.5	1.5	6.1
$\Delta g_1^{\rm Z}$	651.6	315.0	14.7	5.3	35.8	38.1
$\Delta\kappa_\gamma$	1165.0	15.0	1.4	0.9	11.9	4.8
λ_γ	156.1	20.3	1.0	1.2	3.0	12.1
$\Delta\kappa_{\rm Z}$	382.9	28.6	2.5	1.5	5.6	8.7
λ_Z	79.4	10.4	0.5	0.8	1.6	11.5
g_4^Z	86.2	4.2	5.8	2.8	6.5	85.8
g_5^Z	602.4	160.4	15.6	3.5	23.4	27.7
$\tilde\kappa_Z$	2.9	39.7	8.7	1.4	9.7	64.9
$\tilde\lambda_Z$	16.3	2.9	2.9	0.6	3.0	11.4

(a) 500 GeV, no polarization

coupling	ISR 100 %	beamstrahlung 100 %	$M_{\rm W}$	$E_{\rm beam}$	systematic[a] error	statistic error
$\Delta g_1^{\rm Z b}$	32.3	3.5	1.6	0.5	1.7	4.5
$\Delta\kappa_\gamma{}^{\rm b}$	116.1	3.7	1.1	0.3	1.7	3.1
$\lambda_\gamma{}^{\rm b}$	9.6	0.1	0.4	0.2	0.5	2.8
$\Delta g_1^{\rm Z}$	7.7	2.5	11.2	3.4	11.7	39.0
$\Delta\kappa_\gamma$	177.8	3.7	0.9	0.3	2.0	2.6
λ_γ	8.3	0.2	0.9	0.2	0.9	5.2
$\Delta\kappa_{\rm Z}$	36.6	3.5	1.8	0.5	1.9	4.9
λ_Z	5.9	0.3	0.8	0.3	0.9	5.1
g_4^Z	0.2	2.1	2.8	1.2	3.1	41.8
g_5^Z	14.9	8.5	0.8	1.6	2.0	28.5
$\tilde\kappa_Z$	2.5	0.2	5.1	2.5	5.7	29.6
$\tilde\lambda_Z$	2.9	0.1	0.4	0.3	0.5	4.9

(b) 800 GeV, no polarization

[a]Quadratic sum of all systematic errors, assuming 1 % of ISR error and 10 % of beamstrahlung error.
[b]With $\mathrm{SU}(2)_L \times \mathrm{U}(1)_Y$ relations.

Table 7: Estimated systematic error ($\times 10^{-4}$) for different systematic uncertainties.

parameter	$\mathcal{P}^-$	stat error	$\mathcal{P}^-/\mathcal{P}^+$	stat. error
Δg_1^{Z}[a]	36.3	4.3	14.8	2.8
$\Delta\kappa_\gamma$[a]	15.5	4.2	21.9	3.1
λ_γ[a]	10.5	5.1	24.3	4.3
Δg_1^{Z}	134.2	24.8	74.5	15.5
$\Delta\kappa_\gamma$	21.8	4.1	18.7	3.3
λ_γ	21.4	8.2	34.8	5.9
$\Delta\kappa_{\mathrm{Z}}$	44.2	5.0	16.9	3.2
λ_Z	9.1	8.9	39.4	6.7
g_4^Z	680.6	79.9	92.7	45.9
g_5^Z	242.3	22.8	163.8	16.5
$\tilde{\kappa}_Z$	50.9	50.6	169.1	39.0
$\tilde{\lambda}_Z$	64.1	10.3	23.2	7.5

(a) 500 GeV

parameter	$\mathcal{P}^-$	stat error	$\mathcal{P}^-/\mathcal{P}^+$	stat. error
Δg_1^{Z}[a]	5.2	2.7	9.0	1.8
$\Delta\kappa_\gamma$[a]	10.1	2.3	17.0	1.9
λ_γ[a]	1.9	3.1	0.4	2.6
Δg_1^{Z}	30.6	21.9	32.6	12.6
$\Delta\kappa_\gamma$	8.1	2.2	13.0	1.9
λ_γ	5.6	5.0	2.7	3.3
$\Delta\kappa_{\mathrm{Z}}$	5.4	2.9	9.5	1.9
λ_Z	1.9	4.7	1.8	3.0
g_4^Z	32.5	31.8	15.7	18.3
g_5^Z	7.5	31.8	5.2	14.4
$\tilde{\kappa}_Z$	20.1	24.1	6.7	14.3
$\tilde{\lambda}_Z$	1.3	4.4	0.9	3.0

(b) 800 GeV

[a] With $\mathrm{SU}(2)_L \times \mathrm{U}(1)_Y$ relations.

Table 8: Estimated systematic errors ($\times 10^{-4}$) from uncertainties in the polarization measurement compared with the expected statistical error.

polarization	$\mathcal{P}^- = \mathcal{P}^+ = 0$		$\mathcal{P}^- = 80\,\%,\ \mathcal{P}^+ = 0$		$\mathcal{P}^- = 80\,\%,\ \mathcal{P}^+ = 60\,\%$	
energy[GeV]	500	800	500	800	500	800
luminosity[fb^{-1}]	500	1000	500	1000	500	1000
$\Delta\alpha_2$	1.771	2.078	0.329	0.127	0.123	0.090
$\Delta\alpha_3$	0.935	1.004	0.143	0.071	0.083	0.048
$\text{cor}(\alpha_2, \alpha_3)$	-0.993	-0.998	-0.755	-0.682	-0.343	-0.547
Λ_2^* [TeV]	2.3	2.1	5.4	8.7	8.8	10.3
Λ_3^* [TeV]	3.2	3.1	8.2	11.6	10.7	14.1

Table 9: Estimated statistical errors ($\Delta\chi^2 = 1.0$) for the strong EWSB parameters α_2 and α_3, assuming $\alpha_1 = 0$. Both parameters are fitted at the same time.

	$3d$	Δg_1^{Z}	$\Delta\kappa_\gamma$	$\Delta\kappa_{\mathrm{Z}}$
Δg_1^{Z}	24.0	1.000	-0.133	-0.757
$\Delta\kappa_\gamma$	3.4		1.000	0.143
$\Delta\kappa_{\mathrm{Z}}$	4.9			1.000

(a) 500 GeV

	$3d$	Δg_1^{Z}	$\Delta\kappa_\gamma$	$\Delta\kappa_{\mathrm{Z}}$
Δg_1^{Z}	13.5	1.000	-0.147	-0.364
$\Delta\kappa_\gamma$	2.1		1.000	-0.233
$\Delta\kappa_{\mathrm{Z}}$	2.1			1.000

(b) 800 GeV

Table 10: Expected sensitivity ($\times 10^{-4}$) and correlation matrix for a three parameter fit with both beams polarized (RL+LR).

B Plots

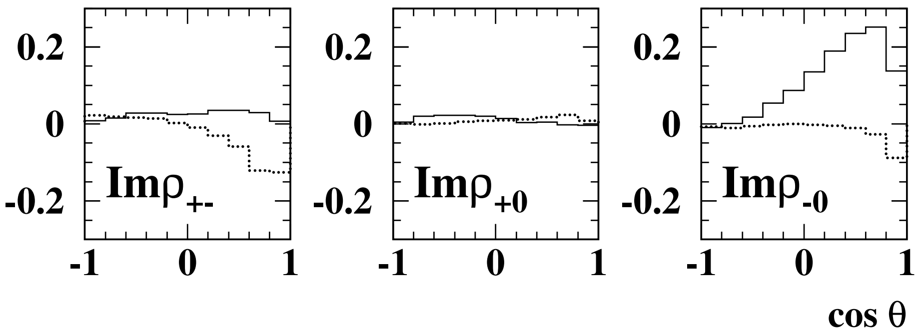

Figure 3: Imaginary parts of the off-diagonal SDM elements for the two anomalous couplings $\tilde{\kappa}_Z = 1$ (solid line) and $\tilde{\lambda}_Z = 1$ (dotted line) at Born-level. For CP conserving couplings the imaginary parts must vanish.

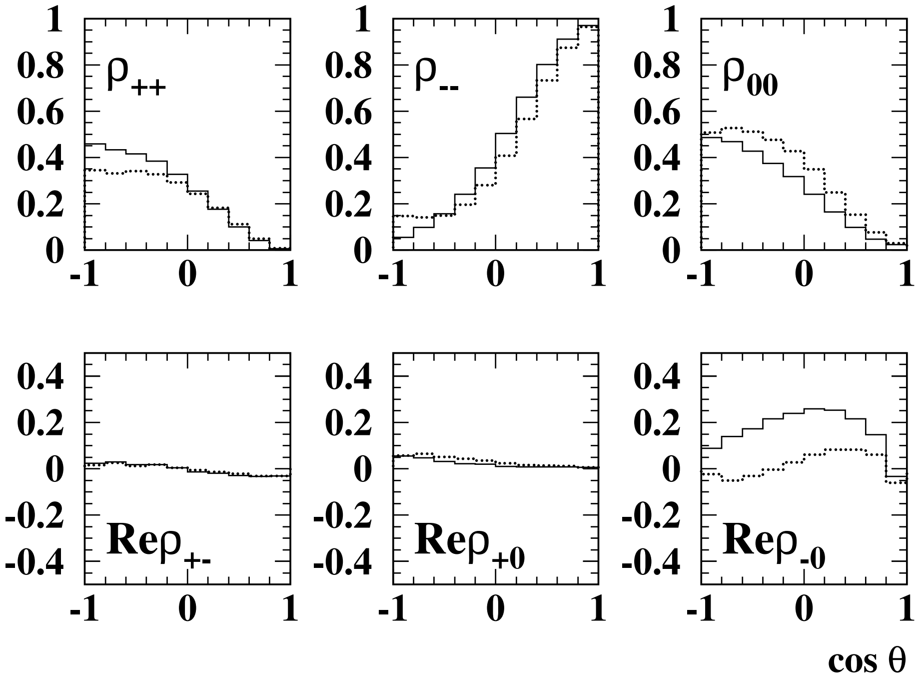

Figure 4: Real part of the SDM elements for the SM (solid line) and an anomalous coupling of $\Delta g_1^Z = 0.1$ (dashed line) at Born-level. The imaginary parts are zero for these couplings.

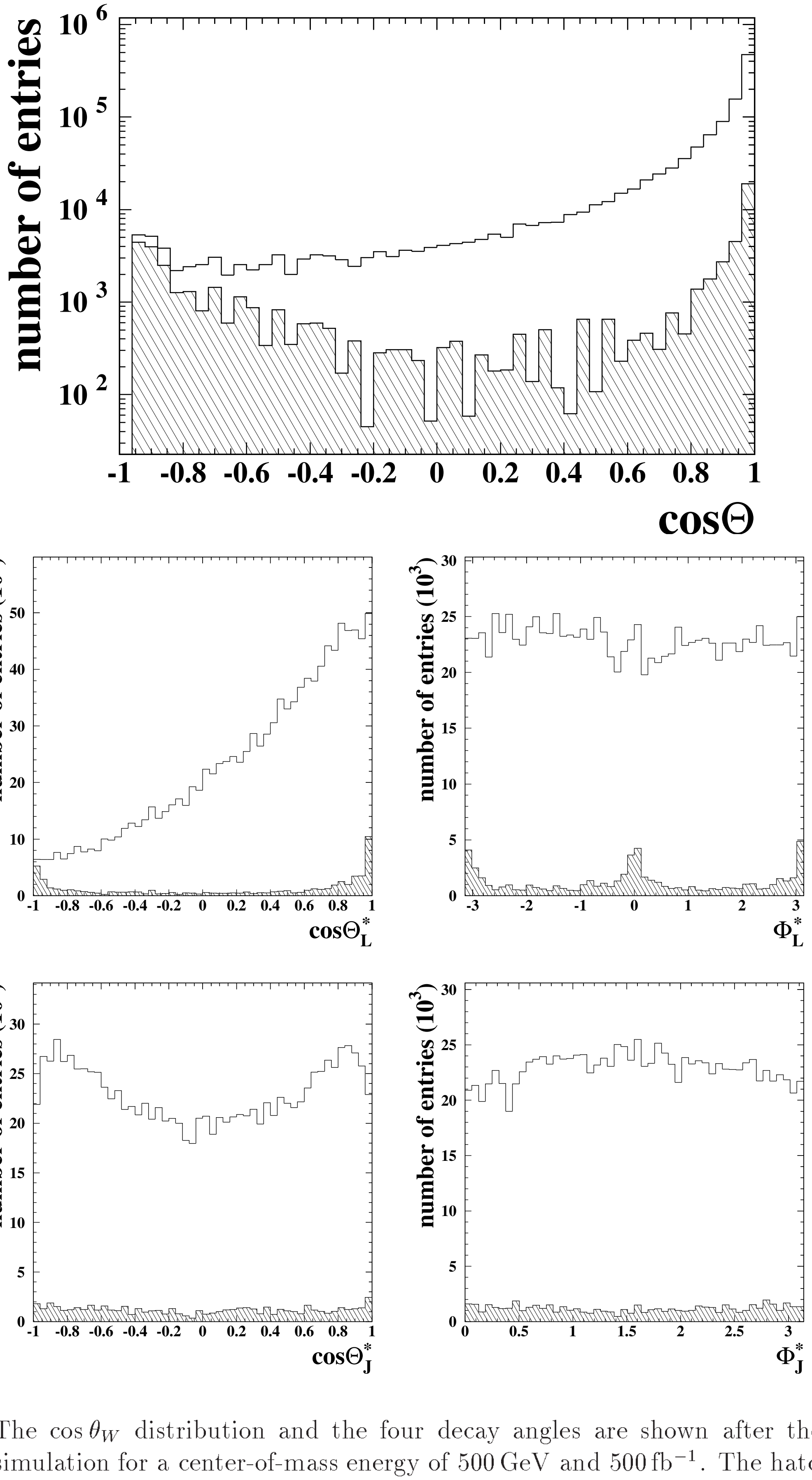

Figure 5: The $\cos\theta_W$ distribution and the four decay angles are shown after the detector simulation for a center-of-mass energy of 500 GeV and 500 fb^{-1}. The hatched curve show the expected background, the open curve the signal, which is plotted on top the background.

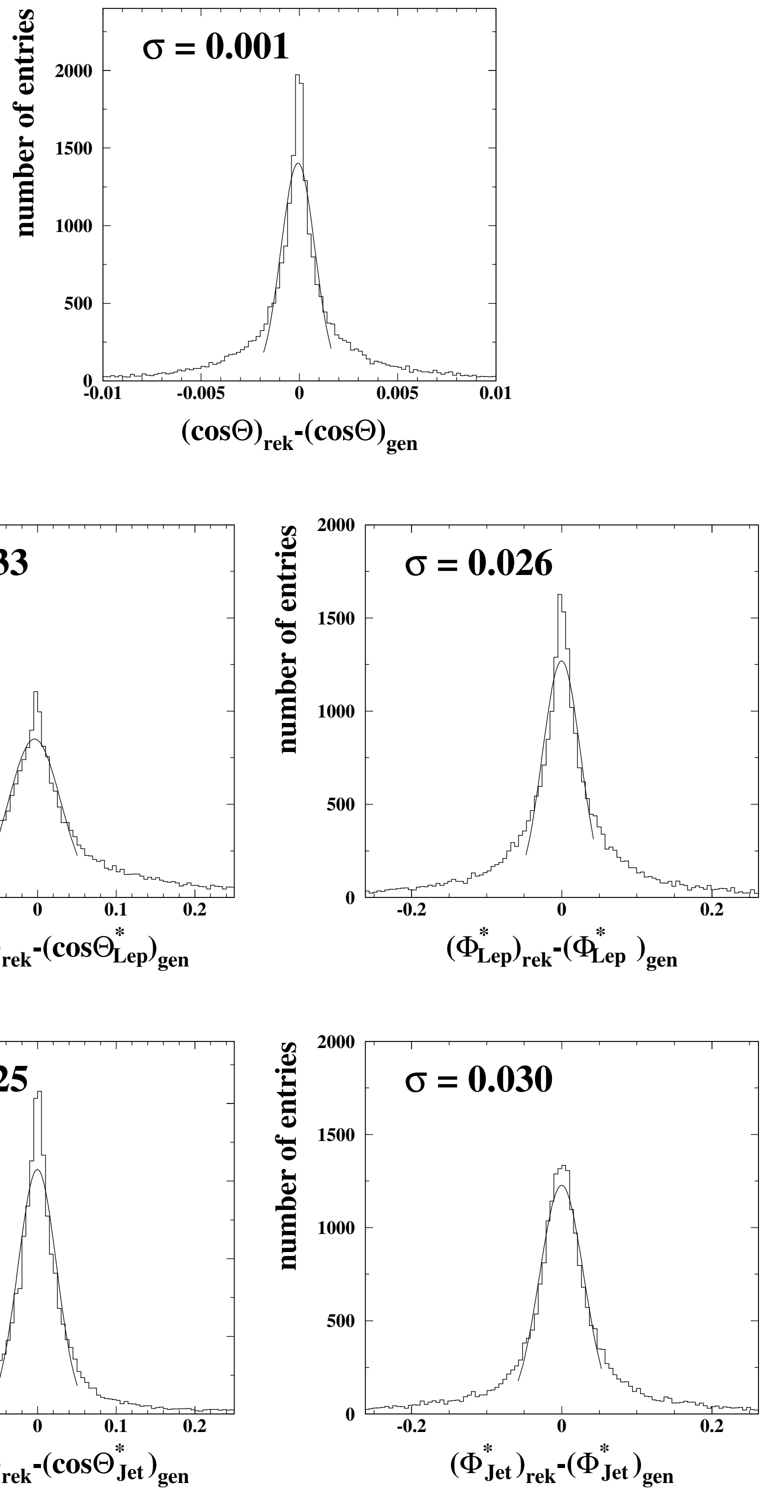

Figure 6: The resolution of $\cos\theta_W$ and the four decay angles are show for a center-of-mass energy of 500 GeV.

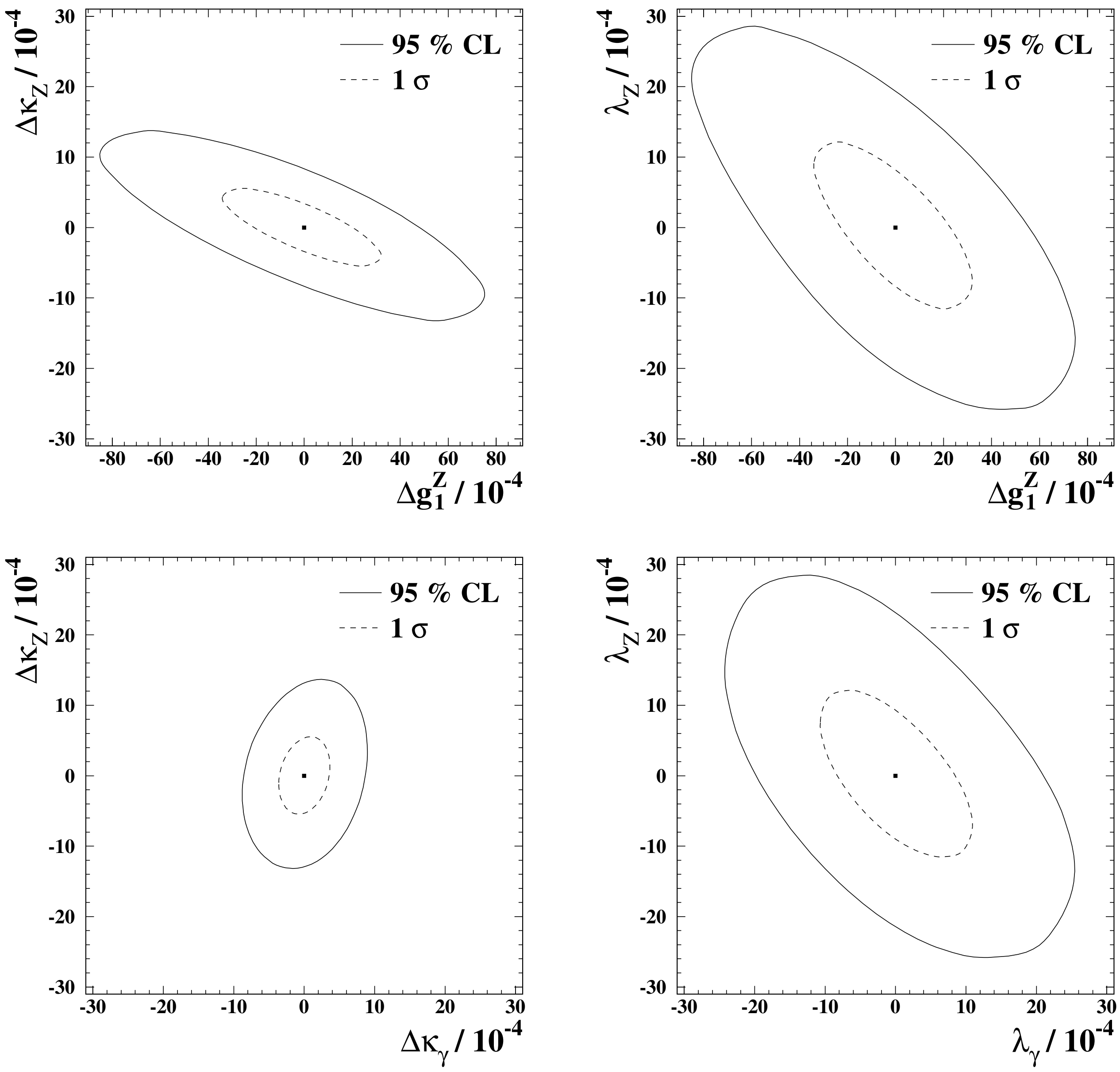

Figure 7: Contour plots of different combinations of couplings for polarized beams at 500 GeV. All five C and P conserving parameter are free to vary. Each point on the lines is a minimum with respect to the other 3 variables. dashed line: $\Delta\chi^2 = 1.0$ and solid line: $\Delta\chi^2 = 5.99$.

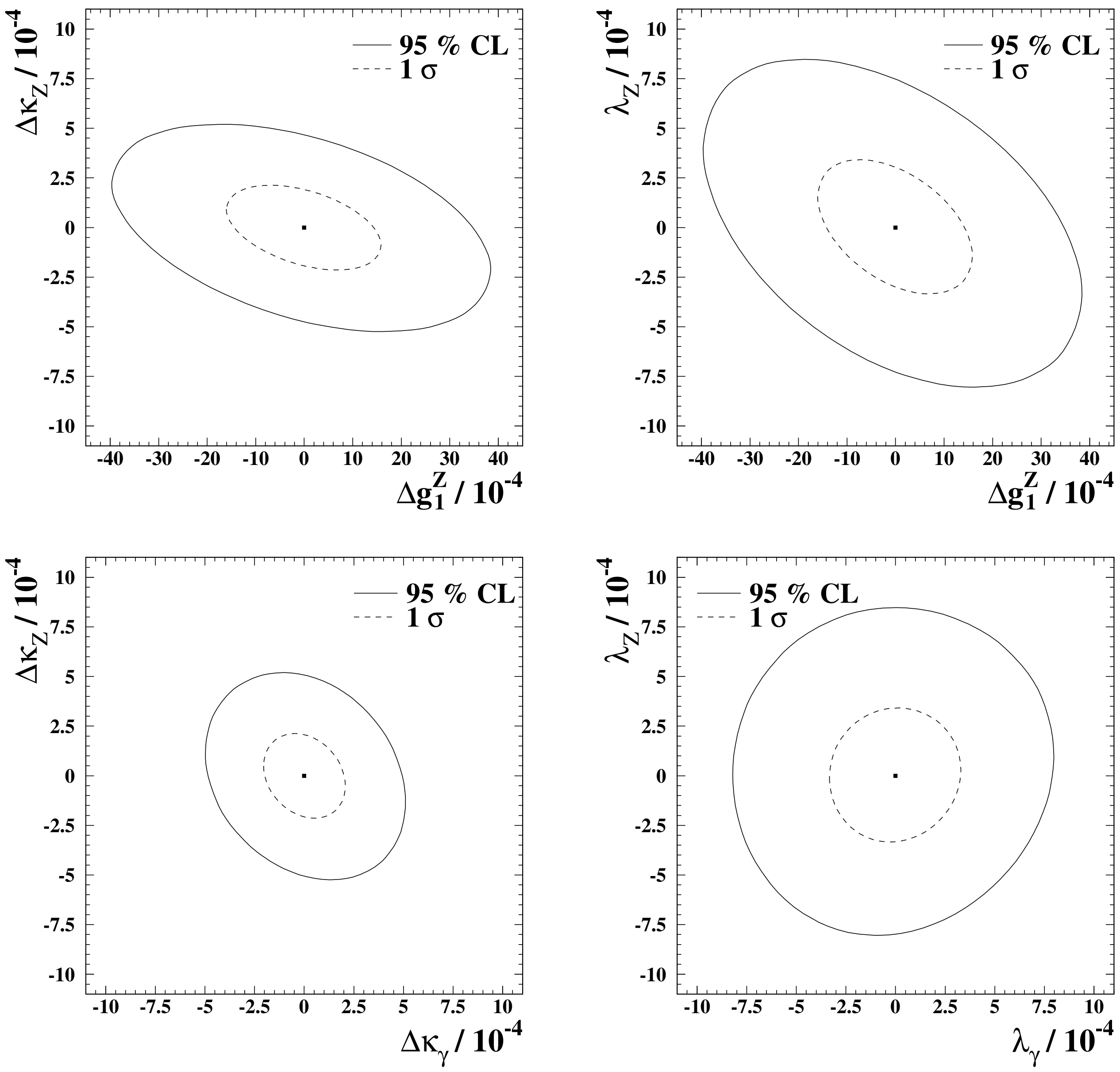

Figure 8: Contour plots of different combinations of couplings for polarized beams at 800 GeV. All five C and P conserving parameter are free to vary. Each point on the lines is a minimum with respect to the other 3 variables. dashed line: $\Delta\chi^2 = 1.0$ and solid line: $\Delta\chi^2 = 5.99$.

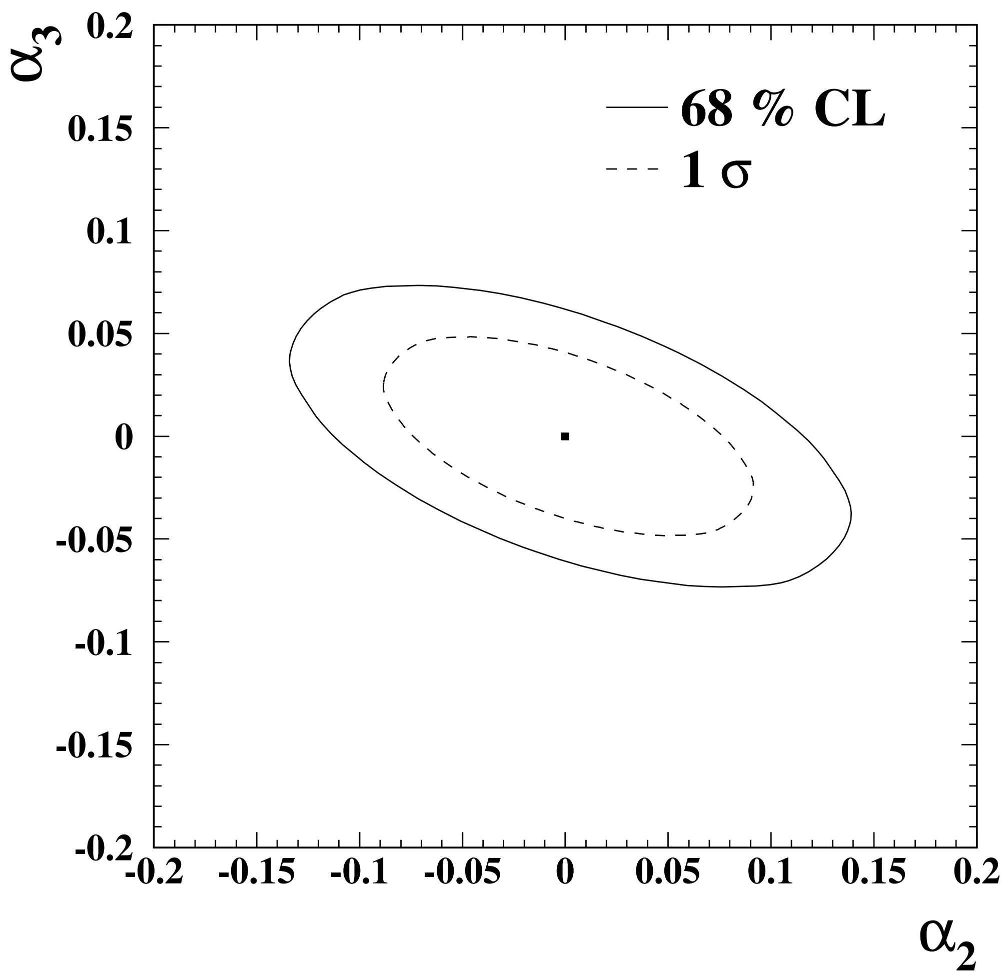

Figure 9: Contour plots of α_2 and α_3 with $\alpha_1 = 0$ for both beams polarized at 800 GeV. The dashed line show the one sigma contour ($\Delta\chi^2 = 1.0$) and the solid line the 68 % confidence level ($\Delta\chi^2 = 2.3$).